Receiver Autonomous Interference Detection

Awele Ndili, *Stanford University*
Dr. Per Enge, *Stanford University*

Presented at the 53rd Annual Meeting of the Institute of Navigation
Albuquerque, New Mexico
June 1997

BIOGRAPHY

Awele Ndili is a Ph.D. student of Mechanical and Electrical Engineering at Stanford University. His work focuses on interference detection and mitigation, and pseudolite signal design. He was a co-recipient of the Best Student Paper award from ION GPS-94, and served as Student Session Chair at ION GPS-96.

Dr. Per Enge is a Research Professor of Aeronautics and Astronautics at Stanford University. He has served as the chair of the Satellite Division of the Institute of Navigation and is the Associate Editor of the Journal of Institute of Navigation.

ABSTRACT

Interference presents a challenge in the use of GPS for aircraft high precision approach, by posing a threat to the accuracy and integrity of the GPS navigation solution. Such interference may result from 'unintentional' sources (such as TV/FM harmonics, Radar, MSS), or may result from hostile (jamming) efforts.

This research focuses on algorithms for on-board interference detection and monitoring. Types of interference considered include CW and broadband, pulsed and continuous. We study the effects of different types of interference on GPS receiver sub-units, including the A/D converter, correlator measurements, the PLL and the DLL. From analysis and simulation we present interference detection algorithms based on the observable effects of the various types of interference on the GPS receiver raw measurements.

Interference detection is based on a combination of the following test statistic - correlator power output, variance of correlator power output, carrier phase vacillation, and AGC control loop gains. The role and benefits of pseudolites in reducing the adverse effects of interference are also discussed.

1. INTRODUCTION

Integrity can be defined as a measure of confidence on the specified accuracy of any given system. Precision GPS applications such CAT II/III aircraft landings place demands for high levels of integrity from a GPS receiver, given the risks involved. Unfortunately RF interference, which occurs naturally in the operating environment of a GPS receiver, can surreptitiously degrade accuracy, thereby compromise the integrity of the receiver. Such interference may be intentional (from an RF jammer) or non-intentional, as would result from channel cohabitance and harmonics from mobile cellular, satellite, TV and FM radio.

Previous approaches [1] have explored ground-based integrity monitoring. However in certain scenarios, interference to on-board receivers may be unobservable from a ground-based monitor. It is therefore desirable for greater reliability to have an independent on-board integrity monitor. Applications such as local and wide area augmentation systems (LAAS and WAAS) stand to benefit from the resulting boost in integrity.

This research presents methods to boost the intrinsic integrity of a GPS receiver by studying the low-level effects of various types of interference on a receiver. Types of interference studied include AWGN, CW and pulsed interference. Tools used for analyses include a software simulation of a GPS receiver, described in section II. Receiver parameters studied include correlator power output, variance of correlator power output, carrier phase vacillation, and adaptive analog-to-digital converter thresholds, defined in section III. Based on results of this study, presented in section III, we demonstrate the effectiveness of these candidate parameters as decision statistics for integrity monitoring.

Finally we also discuss the mitigation of interference through the use of airport-based pseudolites (APLs). APLs provide a strong signal robust in the presence of interference, thereby enhancing continuity over the GPS-only solution.. In addition APLs improve the geometry solution resulting in greater accuracy.

2. SIMULATION SETUP

A GPS receiver simulation was developed as a tool to study the microscopic effects of interference on a the raw receiver measurements. The simulated receiver was modeled after the GEC Plessey open receiver architecture. However by varying any of a wide range of parameters, different kinds of receivers may be simulated.

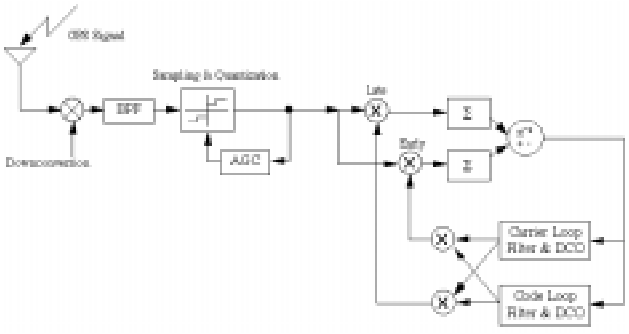

Figure 1: Schematic of Computer Simulation

Figure 1 shows a schematic of the simulated receiver, which is described under subsequent subsections:

i. Signal Generation:

The composite GPS signal is generated for satellites in view for a user located at San Francisco International airport (SFO), based on an almanac downloaded from a real receiver. Weightings are applied as a function of satellite elevation to account for attenuation of signal power of low elevation satellites. Doppler effects are also taken into account for simulated satellites.

ii. Down Conversion:

The RF signal is down-converted via a three stage process to an intermediate frequency of 4.31 MHz. Interference is then added to this analog IF signal, which is then passed through a band-pass filter with a 2 MHz pass band. Output from the filter is sampled and quantized.

iii. Digitization:

Digitization consists of down-conversion by sampling at a frequency of 5.71 MHz, followed by quantization. The adaptive 2-bit analog-to-digital quantizer performs the task of an active gain control (AGC) by varying quantizer thresholds to ensure certain ratios of the output digitized quantities are maintained[1]. Feedback from the quantizer output drives the AGC control.

iv. Correlation:

The final stage in the RF to baseband conversion process consists of correlation with generated early and late inphase and quadrature signals. The correlator output signals, at baseband, are then summed in an integrate-and-dump with an integration time of 1ms. Output from the correlators drive the code and carrier loops. Early and late channels are spaced a quarter chip from prompt.

v. Code and Carrier Tracking:

Early and late correlation channels are combined to form a virtual prompt channel, which feeds the carrier tracking loop. A frequency locked loop (FLL) is used for carrier tracking, offering better performance with interference than conventional phase locked loops [4]. Code tracking employs a second order phase lock loop.

Noise models were developed to generate the following kinds of interference:

- AWGN:
  - bandpass filtered to 2 MHz bandwidth;
  - NSR varied from 0 dB to loss of lock;

- CW:
  - on center (L1) frequency;
  - varied from 0 dB to loss of lock;

- Pulsed broadband:
  - peak AWGN interference power = + 30 dBm;
  - duty cycle varied from 0% to loss of lock;

- Pulsed CW:
  - peak CW interference power = + 30 dBm;
  - duty cycle varied from 0% to loss of lock;

For each run the receiver-under-test (RUT) was first allowed to acquire the GPS signal and attain steady state tracking mode in the absence of interference. The RUT was then subjected to a specified level of each type of interference. The specified level is increased on subsequent runs until the loss-of-lock threshold is exceeded, causing the receiver to go into coast-mode. Results are presented only for the interference regime prior to the onset of coasting, since the coast-mode can be made to trigger an alarm, thereby ensuring integrity.

For the pulsed interference tests, a random pulsing scheme was adopted. Peak pulse power equivalent to +30 dBm was maintained, and pulse duty cycle varied to achieve varied loading.

It was necessary in all runs to add some nominal level of 'background' AWGN to the input signal corresponding to

[1] See GEC Plessey GP2010 RF Front End document sheet.

the receiver thermal noise floor, in order to keep the tracking loops operational.

3. RESULTS

3.1 Introduction

A summary of the simulation runs is shown in table 1 below. The parameters investigated are defined below.

Cause	Effects	
	Observable	**Unobservable**
AWGN	Correlator Power Output	Pseudorange Error
CW Interference	Correlator Power Output Variance	
Pulsed Broadband	Carrier Phase Vacillation	
Pulsed CW Interference	AGC Gains	

Table 1: Summary of Runs

3.1.1 Correlator Power Output

The correlator power output (SNR_{pc}) is a figure computed in the receiver which gives an indication of the average post-correlation signal to noise ratio. It is computed from equation 1 below:

$$\text{Correlator Power Output} = \frac{I^2 + Q^2}{\text{Expected Noise Floor}} \qquad (1)$$

where I and Q are the 1ms-averaged in-phase and quadrature prompt correlator signal. For the results discussed below, the correlator power output shown is averaged over 1 second immediately after introduction of interference.

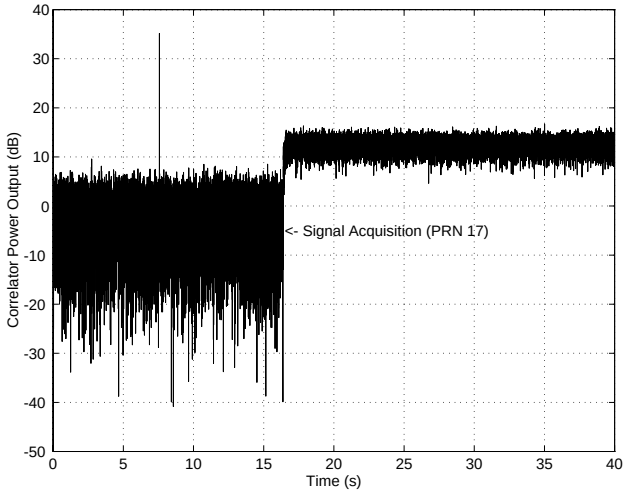

Figure 2: Correlator Power Output for a GPS Receiver

Figure 2 shows the SNR_{pc} for a single channel of a real receiver (GEC Plessey GPS card) immediately before and after acquisition of satellite PRN 17. The figure shows a step increase in the SNR_{pc} and a reduction in its variance following signal acquisition. We observe that the level and variance of the SNR_{pc} are functions of noise in the signal, and therefore are candidates for integrity monitor statistics.

3.1.2 Carrier Phase Vacillation

Carrier phase vacillation provides a measure of the variance or jitter in carrier phase measurements from one measurement epoch to the next, and is defined here as:

Carrier Phase Vacillation =
time average[abs{Carrier Phase_i - Carrier Phase_{i-1}}]

where i is the 1ms epoch index. The carrier phase referenced above is computed from the arctangent of inphase and quadrature phase measurements. Averaging is performed over 1 second immediately following the introduction of interference. Large ($\pm$ 180°) phase swings such as may result from data bit changes, are taken into account and do not affect the computed time average. Carrier phase vacillation results are presented in degrees.

Figure 3 shows the carrier phase of a GPS receiver with a FLL carrier tracking loop over about a half second period. The figure shows the 180 degree flips in the IQ phasor for data bit changes. Carrier phase vacillation computed for this case is 11 degrees. We observe that this quantity is a function of noise/interference, and therefore a candidate integrity statistic.

Note that receiver clock noise as well as interference contribute to vacillations in carrier phase measurement. This study however focuses only on the contribution of interference.

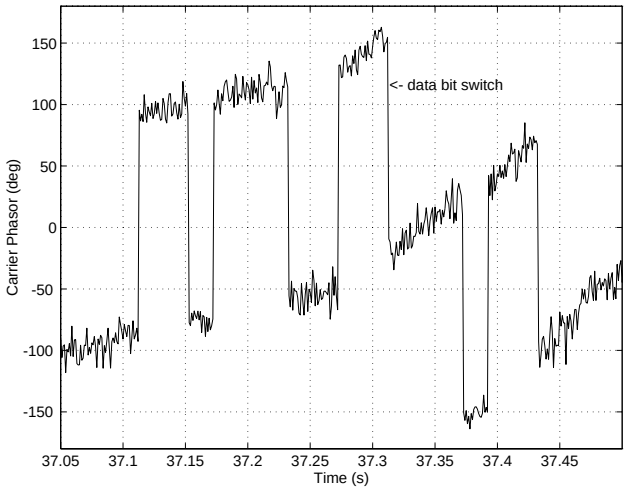

Figure 3: Carrier Phase for a GPS Receiver with a FLL Carrier Tracking Loop

3.1.3 AGC Gains

The control loop of the active gain controller (AGC), located on the signal down-conversion/digitization path, acts by adjusting the threshold levels (r1, r2 an r3 in the figure below) of the 2-bit adaptive analog-to-digital converter to maintain a specified ratio of digitized signal output levels. In this application, the quantizer threshold level is therefore synonymous with AGC gain and is the quantity shown in the results.

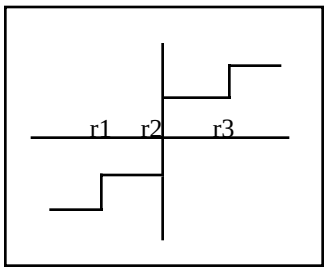

2-Bit Quantizer (AGC)

For an RF signal r2=0, and usually r3=-r1. Included results show averaged values of r3.

3.2 Effect of Interference on Pseudorange

The effect of interference on raw pseudorange measurements, unobservable in the normal operation of a receiver, is shown in figure 4. From figure 4a it can be seen that for C/N_o values less than 40 dB-Hz there is a distinct growth in pseudorange error as the level of interference increases, for both AWGN and CW interference. Figure 4b shows a similar result for pulsed interference, with the marked interference/pseudorange error correlation for duty cycles greater than 20%. Figure 4 also shows the consequences of CW interference to be somewhat more severe than for AWGN within same regime (for non-pulsed interference). This is to be expected from the intrinsic characteristics of spread spectrum decorrelation. A comparison with theoretical prediction from covariance analysis (see solid line on figure 4a) shows the close match between theory and simulation.

3.3 Candidate Integrity Monitor Decision Statistics

Knowledge of the effect of interference on observable parameters provides important insight into how well such parameters will serve as integrity monitor decision statistics. This section justifies the selection of our four decision statistics by presenting results of direct comparison of each test statistic with all four types of interference (see table 1).

Figure 5 shows the performance of correlator power output (SNR_{pc}) with interference. There is a monotonic decrease in SNR_{pc} as interference levels increase, again with the effects of CW appearing more severe in the non-pulsed tests. Figure 5b shows a linear decrease in SNR_{pc} as pulse duty cycle increases. With pulsed CW interference the receiver goes into coast mode at a duty cycle of 68%, 22% lower than with pulsed wideband noise.

The variance of the correlator power output increases with increase in interference, as can be seen from figure 6, for both AWGN and CW, pulsed and non-pulsed. For C/N_o values less than 40 dB-Hz non-pulsed CW interference produces more severe variations in SNR_{pc} (see figure 6a).

Figure 7 shows a well defined increase in carrier phase vacillation with increasing interference, with a steeper increase for C/N_o values less than 40 dB-Hz non-pulsed (figure 7a).

AGC gains correlate directly with interference levels, as seen from figure 8. Again the severity of CW interference can be seen in figure 8a for non-pulsed interference, as CW interference produces higher threshold levels, corresponding to lower SNR_{pc}. Figure 8b shows that pulsed CW interference produces the same threshold effect as with pulsed AWGN, for the +30 dBm peak pulse interference power used in the simulations.

3.4 Interference Detection

The objective of integrity monitoring is to reliably detect normally unobservable but detrimental effects of interference, in our case pseudorange error, from observation of our chosen test statistic. A good decision statistic should therefore correlate closely with increasing levels of interference and deteriorating pseudorange accuracy. In addition the decision statistic should be insensitive to kinds of interference in order to be robust.

Figures 9 through 12 show the observable quantities discussed above in use as decision statistic to detect degradation in pseudorange accuracy with AWGN and CW interference, pulsed and non-pulsed. An arbitrary pseudorange error protection limit of 2 meters is chosen to enable the loose definition of the regions of normal operation, missed detection, false alarm and normal detection. . A linear least square error curve-fit is shown on each plot which shows in all cases a distinct correlation between pseudorange error and all four test statistics. A measure of how closely each test statistic fits its line of least squares fit can be seen from the standard deviations from this line, shown in column 6 of tables 2 and 3. AGC gains and correlator power output show the strongest correlation with minimal spread (σ=0.55m to 0.67m). In all cases the standard deviation

of each test statistics from its linear least squares fit curve is less than 1.2 meters

Tables 2 and 3 show summarized decision statistic results, with percentages of incidents of false alarm (FA), missed detection (MD), normal operation (NO) and normal detection (ND). The definitions of these regions and results were obtained heuristically by the following procedure:

i. Pseudorange error limit was fixed at 2m (horizontal line);

ii. The decision statistic threshold (vertical line) was then chosen such that there was zero incidence of missed detection.

iii. With all 4 regions thus defined, incidents of false alarm, normal operation and normal detection are counted to provide a measure of the effectiveness of the test statistic.

Note that this choice of statistic threshold level is by no means optimized, and is only used here to provide a measure of the effectiveness of each candidate decision statistic. Also note that a real statistic may include margins around the transition boundaries to account for border-line interference and pseudorange error situations, which are present in our simulation as interference is introduced at low levels and gradually ramped up. The result in our case is that our definition of a false alarm region is extremely conservative, and produces a higher false alarm counts than would occur in actual receiver operation.

From tables 2 and 3, results for correlator power output show that 97% (and 98.8% for pulsed interference) of all points lie in regions of normal operation and normal detection. Also the 3% (1.2% pulsed) that fall in the false alarm region lie very close to the border between the regions of normal operation and detection (see figures 9a and 9b). This indicates an intermediate level of both interference and pseudorange error, consistent with the performance of a good test statistic. These results suggest reliability with the use of correlator power output as a test statistic.

	MD	FA	NO	ND	σ(m)
Correlator Power Output	0.0%	3.0%	56.7%	40.3%	0.60
Correlator Power Output Std. Dev.	0.0%	1.5%	58.2%	40.3%	1.01
Carrier Phase Vacillation	0.0%	10.4%	49.3%	40.3%	0.70
AGC Gain	0.0%	1.5%	58.2%	40.3%	0.55

Table 2: Results Summary, CW and AWGN Interference

	MD	FA	NO	ND	σ(m)
Correlator Power Output	0.0%	1.2%	48.2%	50.6%	0.67
Correlator Power Output Std. Dev.	0.0%	3.7%	45.7%	50.6%	0.80
Carrier Phase Vacillation	0.0%	2.5%	46.9%	50.6%	1.11
AGC Gain	0.0%	2.5%	46.9%	50.6%	0.55

Table 3: Results Summary, Pulsed CW and AWGN Interference

This result pattern is repeated for standard deviation of correlator power output, carrier phase vacillation, and AGC gain, with counts for normal operation plus detection ranging from worst case 89.6%, non-pulsed detection via carrier phase vacillation, to 98.5%, for the test statistics: AGC gain and correlator power output standard deviation, operating in a non-pulsed environment. Again in all cases the 'false alarm' points lie very close to normal detection / normal operation boundaries.

Also consider the *crossover point*, defined as the value of a decision statistic at the intersection of the horizontal 2-meter pseudorange error line and the linear least squares fit line. The crossover point defines another candidate value for a decision statistic threshold based on its least square error trend. Comparing crossover points over different types of interference for the same test statistic gives an indication of the robustness of the chosen statistic over different types of interference.

Table 4 shows crossover values for all four candidate decision statistic, for pulsed and non-pulsed interference. Also shown on the table is the maximum range of values of each statistic over the entire interference regime, and the percentage difference in crossover values for pulsed and non-pulsed interference, normalized by each parameters maximum range.

	Crossover Points		Value	Percent
	Continuous	Pulsed	Range	Difference
Correlator Power Output	14.97	14.95	28.75	0.07%
Correlator Power Output Std. Dev.	1.99	1.85	8.02	1.81%
Carrier Phase Vacillation	10.99	10.09	77.97	1.15%
AGC Gain	6.88	43.99	179.96	20.62%

Table 4: Crossover points, Pulsed and Non-pulsed CW and AWGN Interference

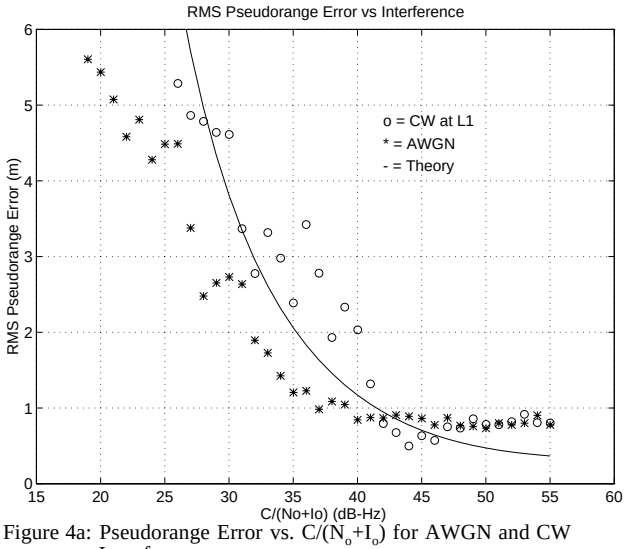

Figure 4a: Pseudorange Error vs. $C/(N_o+I_o)$ for AWGN and CW Interference

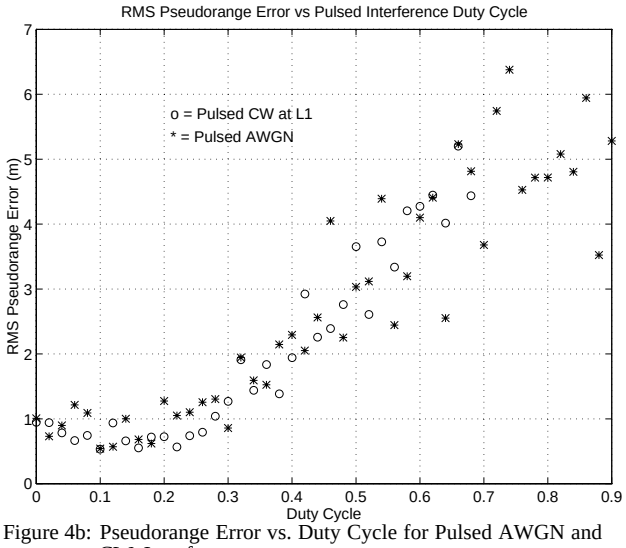

Figure 4b: Pseudorange Error vs. Duty Cycle for Pulsed AWGN and CW Interference

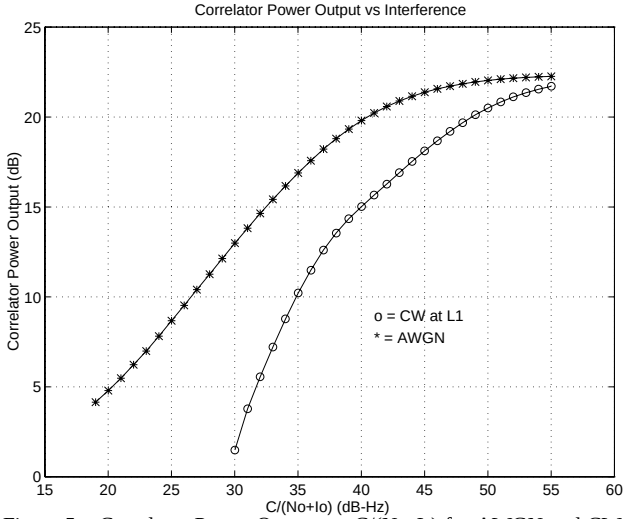

Figure 5a: Correlator Power Output vs. $C/(N_o+I_o)$ for AWGN and CW Interference

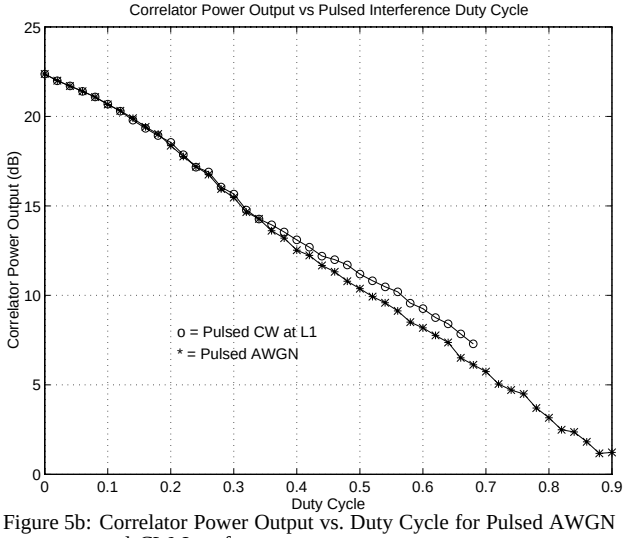

Figure 5b: Correlator Power Output vs. Duty Cycle for Pulsed AWGN and CW Interference

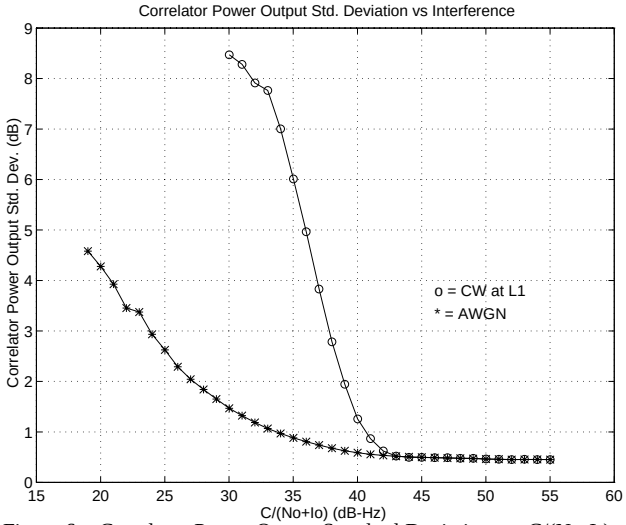

Figure 6a: Correlator Power Output Standard Deviation vs. $C/(N_o+I_o)$ for AWGN and CW Interference

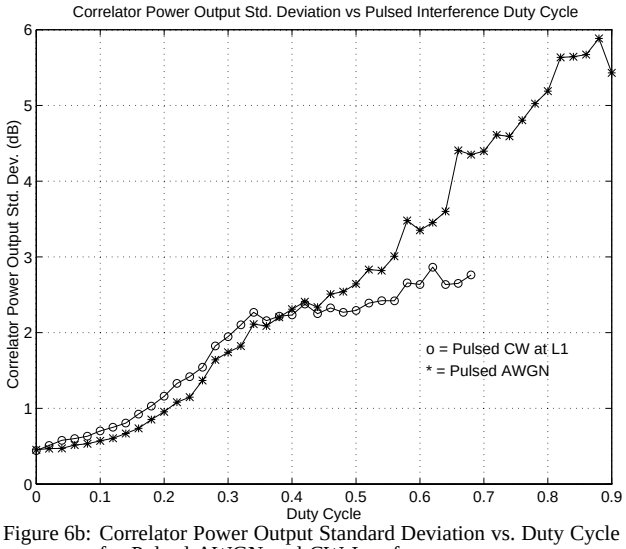

Figure 6b: Correlator Power Output Standard Deviation vs. Duty Cycle for Pulsed AWGN and CW Interference

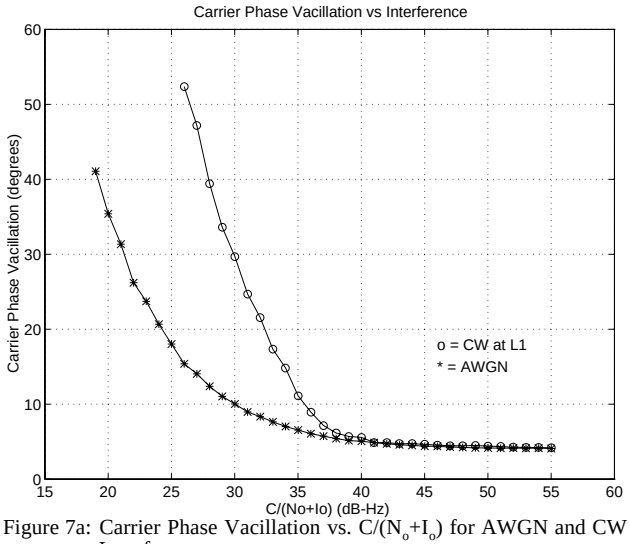

Figure 7a: Carrier Phase Vacillation vs. $C/(N_o+I_o)$ for AWGN and CW Interference

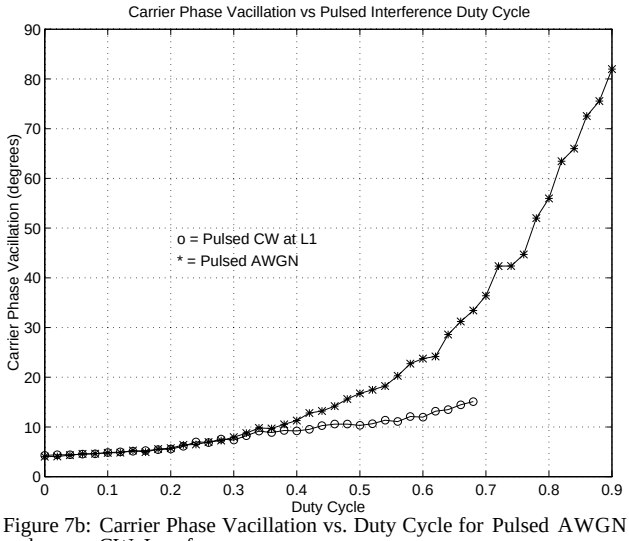

Figure 7b: Carrier Phase Vacillation vs. Duty Cycle for Pulsed AWGN and CW Interference

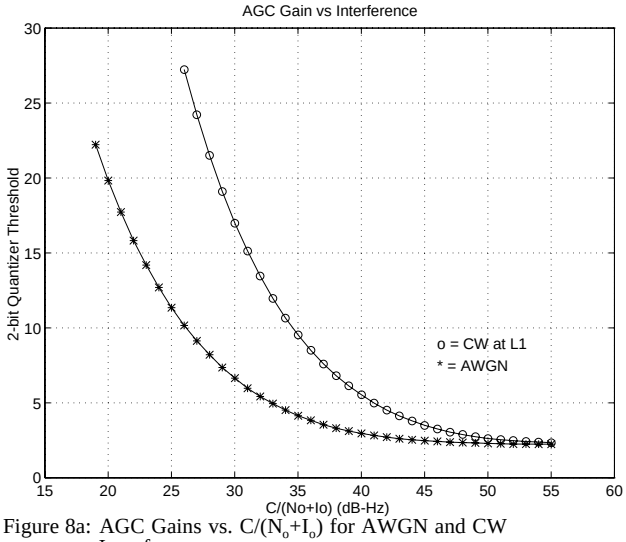

Figure 8a: AGC Gains vs. $C/(N_o+I_o)$ for AWGN and CW Interference

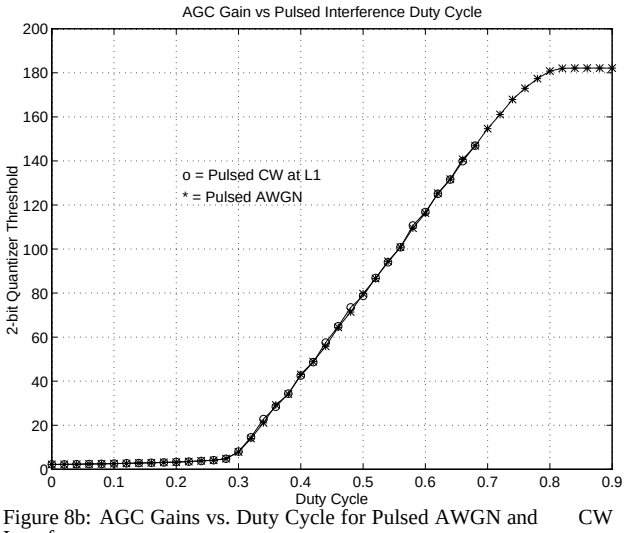

Figure 8b: AGC Gains vs. Duty Cycle for Pulsed AWGN and CW Interference

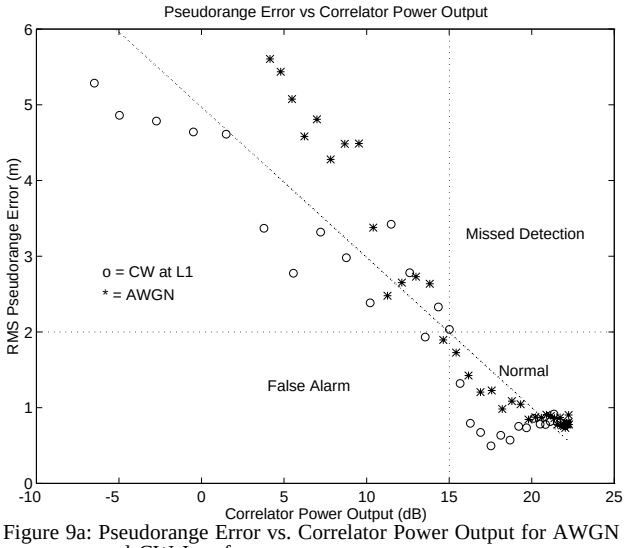

Figure 9a: Pseudorange Error vs. Correlator Power Output for AWGN and CW Interference.

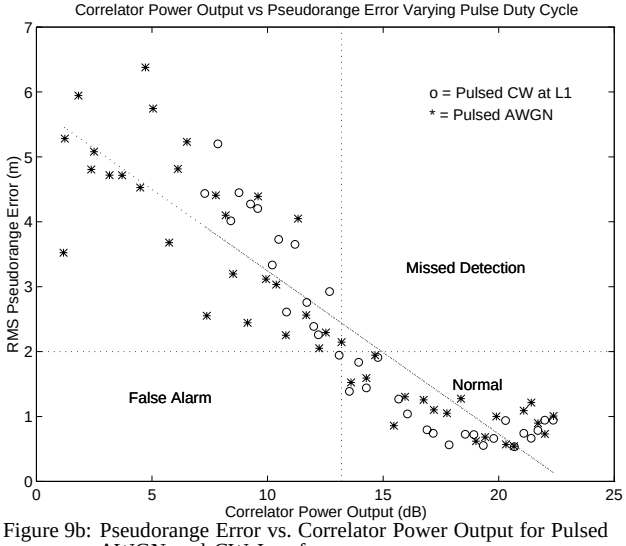

Figure 9b: Pseudorange Error vs. Correlator Power Output for Pulsed AWGN and CW Interference.

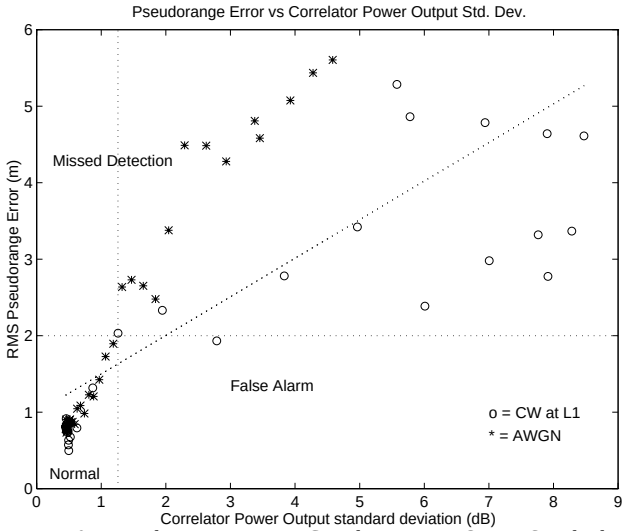

Figure 10a: Pseudorange Error vs. Correlator Power Output Standard Deviation for AWGN and CW Interference.

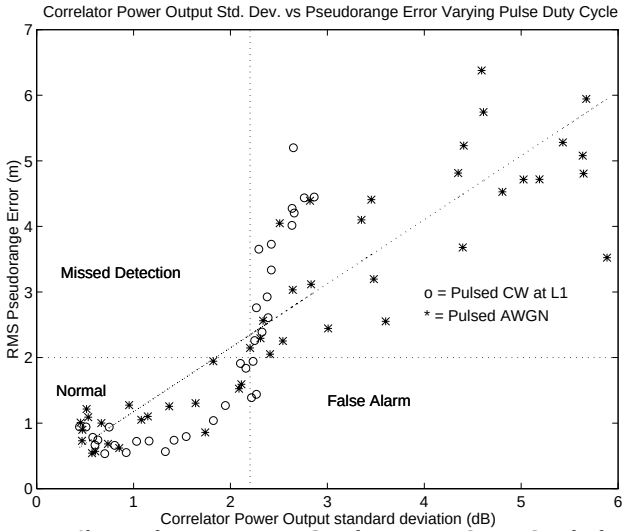

Figure 10b: Pseudorange Error vs. Correlator Power Output Standard Deviation for Pulsed AWGN and CW Interference.

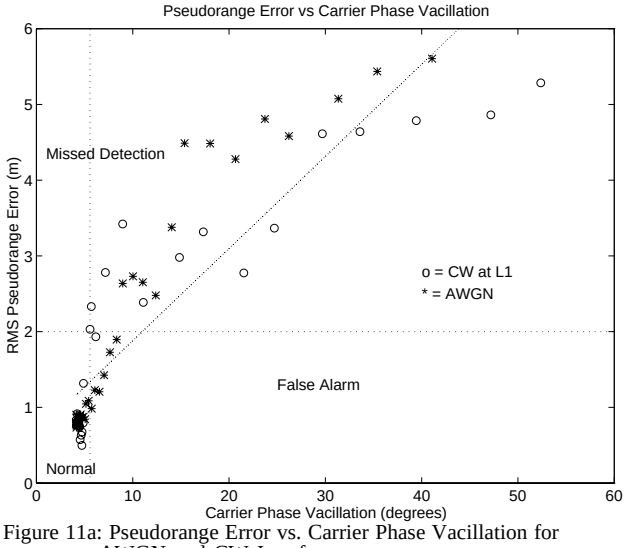

Figure 11a: Pseudorange Error vs. Carrier Phase Vacillation for AWGN and CW Interference.

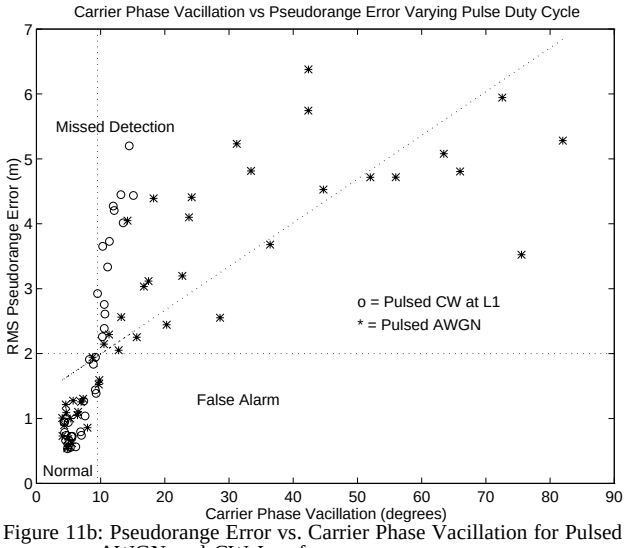

Figure 11b: Pseudorange Error vs. Carrier Phase Vacillation for Pulsed AWGN and CW Interference.

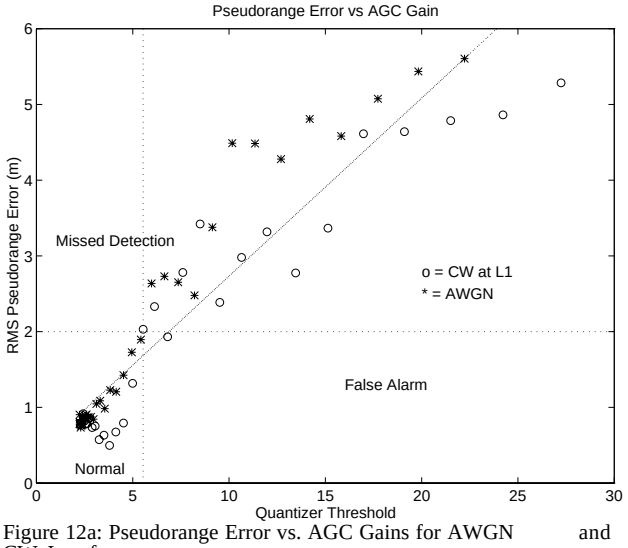

Figure 12a: Pseudorange Error vs. AGC Gains for AWGN and CW Interference.

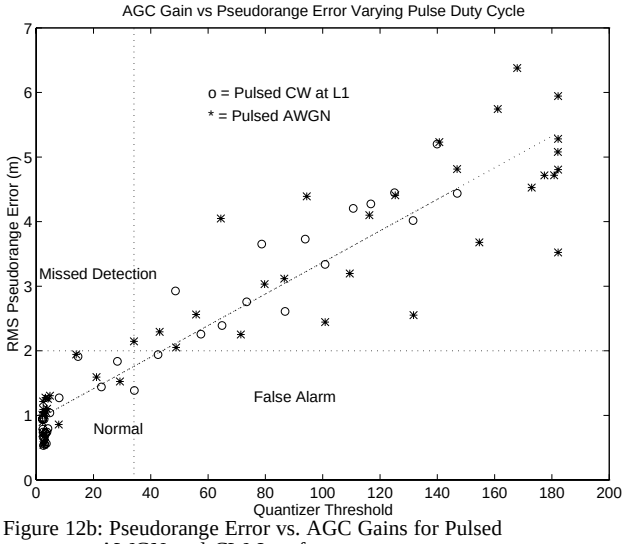

Figure 12b: Pseudorange Error vs. AGC Gains for Pulsed AWGN and CW Interference.

As seen from table 4, correlator power output is most robust to variations in interference type, as its crossover point hardly changes for continuous and pulsed interference (0.07% change). Carrier phase vacillation and standard deviation of correlator power output both show robustness with threshold changes of less than 2%. Least robust to different kinds of interference is the AGC gain, as is to be expected, since under pulsed interference, a fast AGC operates as a pulse suppressant, greatly raising the 2-bit quantizer threshold values (20.62% change).

4. INTERFERENCE MITIGATION VIA USE OF PSEUDOLITES

Airport pseudolites (APLs), while producing pulsed interference, also help to mitigate interference by providing a strong navigation signal impervious to many forms of interference. Figures 13a and 13b below show results of a covariance analysis for no APL - differential GPS only, and for augmentation with 2 intrack APLs providing differential carrier phase measurements.

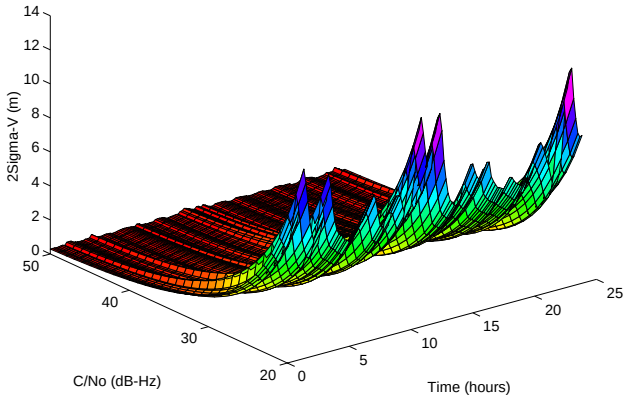

Figure 13a: $2\sigma_v$ vs. $C_{zenith}/(N_o+I_o)$ over time for DGPS

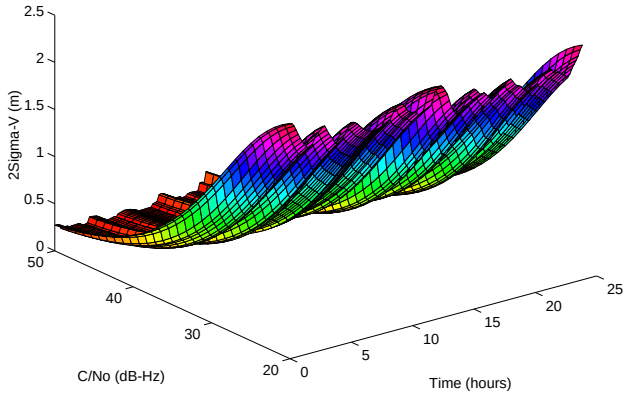

Figure 13b: $2\sigma_v$ vs. $C_{zenith}/(N_o+I_o)$ over time for 2 APLs

APLs are pulsed, each with a 10% duty cycle. Vertical position error, $2\sigma_v$, is shown against $C_{zenith}/(N_o+I_o)$ over a 24 hour period. A 24-satellite almanac is used for receiver location at SFO.

From the figures, it can be seen that the 2-APL solution provides a more robust and reliable solution than DGPS, with a worst case error of 2.5m, compared to 12.8m for DGPS, corresponding to a high interference environment with C/N_o = 20 dB-Hz.

5. CONCLUSIONS

In conclusion we have examined four observable receiver parameters as candidate decision statistic for integrity monitoring, and have demonstrated the reliability and robustness of these parameters. Correlator power output shows best consistent performance under varying levels as well as types of interference. Similar conclusions apply to carrier phase vacillation and standard deviation of correlator power output. AGC gain while showing good consistent performance within either pulsed or non-pulsed interference, produces markedly higher decision threshold values for pulsed interference as a result of its pulse suppression role. While this result may indicate its unsuitability as the single universal decision statistic, it may also be a beneficial resource for the detection of interference type.

In actual operation integrity monitoring may be achieved from a combination of a number of these decision statistics, taking into account each individual performance profile. Also decision threshold selection may be optimized from the use of higher order curve fits, which follow more closely each decision statistic trend.

The use of airport pseudolites provides robustness against interference, weak GPS signal from low elevation satellites, and satellite outages.

ACKNOWLEDGMENTS

The authors gratefully acknowledge the support and assistance of the FAA-Stanford WAAS research grant.

REFERENCES

[1] C. Shively, Y. Lee, "A Position-Domain Ground-Based Integrity Method for LAAS", Institute of Navigation, GPS Technical Meeting, September 1996.

[2] B. Parkinson, J. Spilker, P. Axelrad, P. Enge, *Global Positioning System: Theory and Applications*, AIAA Washington DC, 1996

[3] T. Walter, P. Enge, "Weighted RAIM for Precision Approach", Institute of Navigation, GPS Technical Meeting, September 1995.

[4] Cahn, C. R. et al, "Software Implementation of a PRN Spread Spectrum Receiver to Accommodate Dynamics", IEEE Trans. on Communications, Vol. COM-25, No. 8, August 1977

[5] M. Johnson, R. Erlandson, "GNSS Receiver Interference: Susceptibility and Civil Aviation Impact", Institute of Navigation, GPS Technical Meeting, September 1995.

[6] C. Hegarty, "Analytical Derivation of Maximum Tolerable In-Band Interference levels for Aviation Applications of GNSS", Institute of Navigation, GPS Technical Meeting, September 1996.

[7] B. Parkinson, P. Axelrad, "Autonomous GPS Integrity Monitoring Using the Pseudorange Residual", *Navigation*: Journal of The Institute of Navigation, Vol. 35, No. 2, Summer 1988.

[8] F. Amoroso, "Performance of the adaptive A/D converter in combined CW and Gaussian interference", IEEE Transactions on Communications, Vol. COM-34, No. 3, March 1986.